Marine Micropaleontology 69 (2008) 52–69

Contents lists available at ScienceDirect

Marine Micropaleontology

journal homepage: www.elsevier.com/locate/marmicro

Variations in coccolithophorid production in the Eastern Equatorial Pacific at ODP Site 1240 over the last seven glacial–interglacial cycles

Gatsby-Emperatriz López-Otálvaro [a,*], José-Abel Flores [a], Francisco Javier Sierro [a], Isabel Cacho [b]

[a] Department of Geology, University of Salamanca, Plaza de la Merced s/n, E-37008 Salamanca, Spain
[b] CRG Marine Geosciences, Department of Stratigraphy, Paleontology and Marine Geosciences, University of Barcelona, C/Martí i Franqués, s/n, E-08028 Barcelona, Spain

ARTICLE INFO

Article history:
Accepted 19 November 2007

Keywords:
Coccolithophores
Paleoproductivity
Pleistocene
Coccolith carbonate
Nannofossil accumulation rate (NAR)
Eastern Equatorial Pacific
ENSO

ABSTRACT

The calcareous nannofossil assemblage from ODP Site 1240 in the equatorial upwelling of the Eastern Pacific was analysed for the last 560 Ka. The chronological framework was set with a combination of isotopic stratigraphy, nannofossil biostratigraphy and one paleomagnetic event. Owing to the dominance of selected Noelaerhabdaceae taxa and *Florisphaera profunda*, the *N* index (modified from [Flores, J.A., Bárcena, M.A. y Sierro, F.J., 2000. Ocean-surface and wind dynamics in the Atlantic Ocean off northwest Africa during the last 140 000 years. Palaeogeography, Palaeoclimatology, Palaeoecology 161, 459–478]) was used to investigate the fluctuations of the nutri-thermocline in the Eastern Equatorial Pacific Ocean. This ratio measures the relative proportion of taxa that usually live in the upper photic zone in relation to those that usually thrive in the lower photic zone. Temporal changes in the relative abundances of these species over the last 560 Ka may therefore be related to variability in surface water conditions. Patterns indicated by the *N* index, were supported by the nannofossil accumulation rate and the total $CaCO_3$ coccolith content, allowing identification of four paleoceanographic intervals. Interval 1 (Marine Isotope Stage—MIS 14-8) is characterised by the highest index of paleoproductivity, maximum coccolith accumulation rates and the highest carbonate content, essentially produced by *Gephyrocapsa caribbeanica*. These indicators imply a strengthening of the Southern Hemisphere circulation that allowed enhanced upwelling conditions, possibly related to dominant La Niña-like conditions. Interval 2 (MIS 8-6) displays frequent fluctuations of high *N* index values, in agreement with the slight rise of *F. profunda* and the warm taxa. Both the fall in the nannofossil accumulation rate (NAR) and in the coccolith $CaCO_3$ content were responses to the decrease in *G. caribbeanica* abundance. These events are still associated with high surface productivity related to variations in intensity of the southeast Trade winds and periodically intensified upwelling, conditions related to La Niña-like events with some fluctuations. Interval 3 (MIS 5) is characterised by atypical low *N* values, a low NAR, and a low coccolith $CaCO_3$ content, suggesting that the Southern Hemisphere circulation was reduced and that the upwelling system was weakened, allowing us to infer that an El Niño-like event was the dominant condition. Finally, during Interval 4 (MIS 4-1), the system was reestablished; the *N* index was high again, with some inflections, and correlated with an increase in the NAR and coccolith carbonate. These indicators are related to enhance southeast trades and equatorial currents that favoured cool and nutrient-rich waters, suggesting a La Niña-like condition with some fluctuations.

1. Introduction

In this study we analysed the evolution of calcareous nannofossil assemblages over the last seven glacial–interglacial cycles to elucidate the oceanographic response of the

* Corresponding author.
E-mail address: gatsbyemperatriz@usal.es (G.-E. López-Otálvaro).

0377-8398/$ – see front matter © 2008 Elsevier B.V. All rights reserved.
doi:10.1016/j.marmicro.2007.11.009

Eastern Equatorial Pacific (EEP) to climate change. Calcareous nannofossils, a primarily algal group, are good environmental proxies owing to their temporal and spatial distribution (Brand, 1994), and are hence useful as a tool for paleoceanographic reconstructions. Their highest relative abundances within the phytoplankton occur in warm and oligotrophic waters (Brand, 1994), but their highest absolute abundances occur in eutrophic regions, such as equatorial upwelling regions and on the outer continental shelves (Mitchell-Innes and Winter, 1987; Brand, 1994). The aims of this study are to investigate variations in the nannofossil assemblage, their contribution to carbonate production and export during the last 560 Ka (in order to reconstruct the dynamics of the nutri-thermocline in the EEP) and the influence of the long-term El Niño-like and La Niña-like settings.

The Eastern Equatorial Pacific (EEP) is an area of high productivity associated with seasonal variations of the Trade wind system and with the interannual variability of the ENSO system (El Niño Southern Oscillation, Philander, 1995; Clement et al., 1999; Fedorov and Philander, 2000). The major role of the EEP in the past global climate system has been documented by Chavez and Barber (1987), who stated that this region is responsible for as much as 50% of the global "new production". Long-term changes in paleoproductivity and in the dynamics of the ocean surface currents in the EEP are driven by the Trade wind system (Philander, 1995). Furthermore, the Eastern Pacific is a key part of the El Niño Southern Oscillation. This has two phases, the warm one (El Niño) and the cool one (La Niña), both of which cause oceanographic and atmospheric anomalies around the Earth (e.g. Philander, 1995; Fedorov and Philander, 2000). El Niño events occur in the Pacific when the differences in surface pressure across the tropical Pacific are small and consequently the Trade winds are weak (Fig. 1). Advection and upwelling in the Equatorial Cold Tongue diminish because of the eastward advection of warm nutrient-depleted Western Equatorial Pacific surface waters, thickening the EEP mixed layer and markedly depressing the thermocline and nutricline (Philander, 1995; Fedorov and Philander, 2000). The Equatorial Cold Tongue in the Eastern Equatorial Pacific is a region associated with cool waters, forming a temperature minimum at the equator (Wyrtki, 1981), and with high-oxygen waters (Lukas, 1986). During La Niña events, the differences in surface pressure across the tropical Pacific are unusually large; the Trade winds are intense, and this strengthens advection and upwelling in the Equatorial Cold Tongue, with the subsequent rise of the nutricline and thermocline and a lowering of sea surface temperatures (SST; Philander, 1995; Fedorov and Philander, 2000). During El Niño the warm pool of the Panama Basin moves southward and during La Niña the Equatorial Cold Tongue is markedly enhanced and the nutricline and thermocline rise (Philander, 1995).

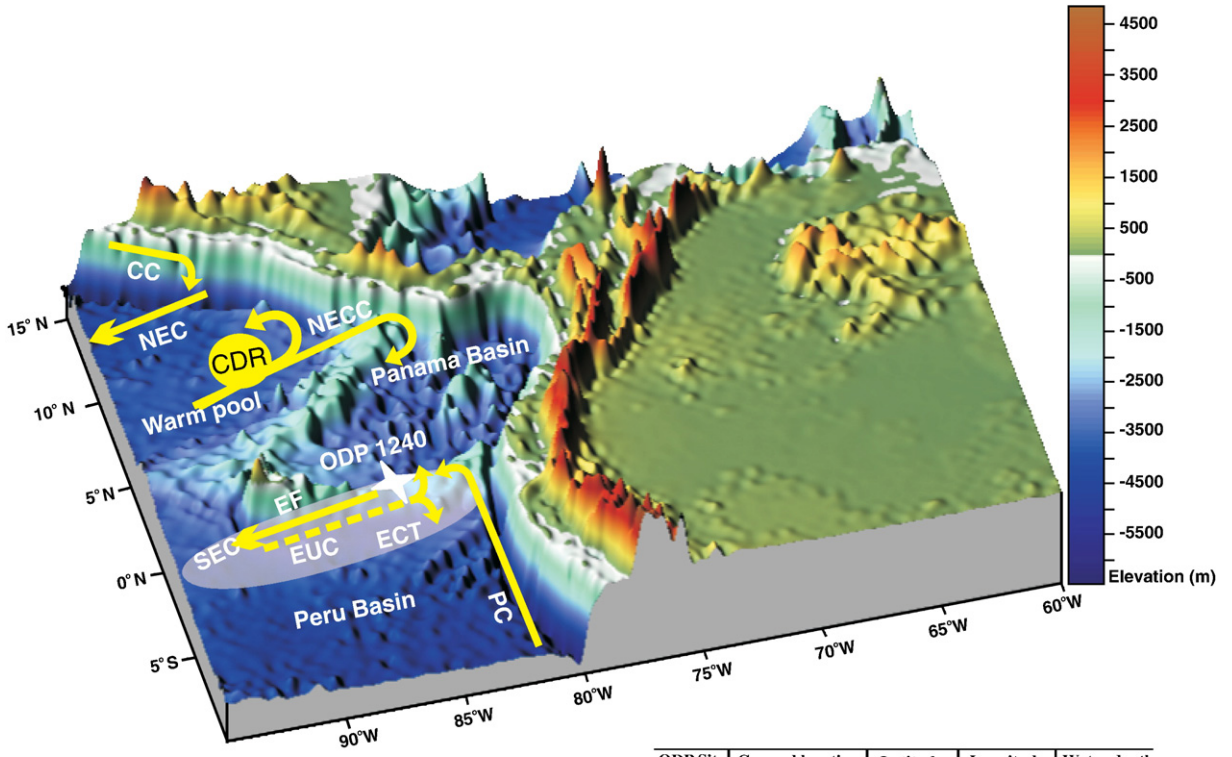

ODP Site	General location	Latitude	Longitude	Water depth
1240	Cocos Ridge (Panama Basin)	0°1.311'N	86°27.258'W	2921 m

Fig. 1. 3-D main surface and subsurface oceanic circulation features in the equatorial upwelling in response to atmospheric dynamics. Colour scale highlighting major bathymetric features (taken from topography database from Smith and Sandwell, 1997). Surface currents are indicated by solid lines and subsurface currents are indicated by dashed lines. PC: Peru Current, SEC: South Equatorial Current, EUC: Equatorial Undercurrent, NEC: North Equatorial Current, CC: California Current, NECC: North Equatorial Counter Current, CDR: Costa Rica Dome, ECT: Equatorial Cold Tongue (Adapted from Fiedler and Talley, 2006; and Kessler, 2006).

2. Oceanographic setting

ODP Site 1240 is situated north of Carnegie Ridge in the equatorial divergence zone, and south of the equatorial front (Mix et al., 2003; Fig. 1). This equatorial front is close to 3°N and forms the boundary between two water masses: the Equatorial Cold Tongue and the warm pool of the Panama Basin. The warm pool is the warm low-salinity tropical surface water associated with the North Equatorial Countercurrent (NECC) (Wyrtki, 1981). The cold tongue is the cold and high-salinity nutrient-rich water south of the front. This tongue comprises the South Equatorial Current (Pak and Zaneveld, 1974; Wyrtki, 1981), the Equatorial Undercurrent (EUC) and the Peru Current (PC) (Pak and Zaneveld, 1974). It is enhanced from August to October and weakened from February to March.

The PC flows northward toward the equator, introducing cool saline, nutrient-rich waters. The PC merges with the SEC in the Galapagos region, feeding the coastal upwelling. The EUC is 100 m thick and flows eastward beneath the SEC, south of 3°N. It is formed of cooler and saltier waters enriched in nutrients that upwell in the equatorial divergence zone (Wyrtki, 1981) and it drives oxygen-rich waters from 150°E to Ecuador at the equator (Helly and Levin, 2004). Equatorial upwelling is attributed to longitudinal divergence induced by the southeast trades and vertical mixing of the EUC (Pak and Zaneveld, 1974; Wyrtki, 1981). Lyle et al. (2002) located the equatorial high-productivity zone, related to the upwelling of nutrient-rich and colder waters, between 1°N and 1°S. The California Current (CC) is driven southward by the northeast trades and feeds the easterly North Equatorial Current (NEC) with cooler and more saline waters. The NECC flows eastward and develops a cyclonic gyre when it reaches the coast of Central America, giving way to a region of upwelling and a shallower thermocline called the Costa Rica Dome and providing westward-flowing surface waters to the NEC (Hoffman et al., 1981) (Fig. 1). The NECC flows eastward from the western equatorial "warm pool" north of 5°N (Wyrtki, 1981).

The trades converge onto the ITCZ, located north of the equator in the EEP. This asymmetry above the EEP was explained by Philander et al. (1996) as being the result of ocean–atmosphere interactions and of the geometry of the American continent. The ITCZ is located over warmer SST associated with the eastward NECC. Precipitation in the Equatorial Cold Tongue is lower than in the northeastern tropical region of the EEP (Philander et al., 1996; Fig. 1). When the southeast trades are fully developed (August to December), the ITCZ is at its northernmost position, at about 10°N; the SEC and the NECC are stronger, and the CC contributes waters to the NEC up to about 20°N. From February to April, the southeast Trade winds are weakened and the northeast trades are most intense. Thus, the ITCZ is at its southernmost position of the year, always north of the equator, causing the lowest surface salinity values and the highest sea surface temperatures (SST) of the year (Philander et al., 1996).

3. Materials and methods

3.1. Sediment and coccolith preparation

The sediments from the upper 52.10 mcd (meter composite depth) of ODP Site 1240 consist of a mixture of biogenic calcite and opal, dominated by nannofossils (~40% to ~80%) and diatoms (~10% to ~40%) (Mix et al., 2003). 145 samples were prepared in order to analyse the calcareous nannofossil assemblage, using the quantitative settling technique of Flores and Sierro (1997). This allows calculation of the abundances of nannofossils per gram of sediment. 0.2 g of dry bulk sediment was diluted in a 10 ml flask with buffered distilled water. Then, this mixture was briefly sonicated (20 s) in an ultrasonic bath. 0.1 ml of the solution was pipetted out and homogenised on a Petri-dish with a coverslip on its bottom. This Petri-dish had previously been filled with buffered distilled water and unflavoured gelatine to ensure uniform distribution of the sediment on the slide. Then, the coverslip was mounted with Canada Balsam on a slide.

Using a polarised Light Microscope (1250×), more than 500 specimens per sample were counted from a variable number of viewing fields. Reworked Miocene, Pliocene and Pleistocene nannofossils were also counted, but were always rare. Additional Scanning Electron Microscope (SEM) analyses were carried out on selected samples using the SEM of the Geological Institute, Kiel. These analyses were used to settle taxonomic aspects and to observe preservation features, confirming a good to moderate preservation of the calcareous nannofossils throughout the site. The species identified are listed in Appendix A.

3.2. Age model and stratigraphy

The age model used in this study is a combination of nine control points of the oxygen isotope record (0–329 Ka; Cacho et al., in prep.), a biostratigraphic event (LAD of *Pseudoemiliania lacunosa*; Flores et al., 2006), and a paleomagnetic datum at 780 Ka (Mix et al., 2003) (Table 1, Fig. 2). The age model for the interval between 0 and 329 Ka was developed at the University of Barcelona, tuning the oxygen isotopic curve of the planktonic foraminifera *Globigerinoides ruber* (white) to the $\delta^{18}O$ record of *G. ruber* (white) of ODP Site 677 of Shackleton et al. (1990) for the last 329 Ka (Cacho et al., in prep.).

Two biostratigraphic events have been identified in ODP Site 1240: the LAD (Last Appearance Datum) of *P. lacunosa* at 44.14 mcd (Flores et al., 2006), and FAD (First Appearance Datum) of *Emiliania huxleyi* at 29.03 mcd (present work), corresponding to 458-Ka (Marine Isotope Stage—MIS 12) and 270-Ka (MIS 8). These events were dated by Thierstein et al. (1977) at 458 Ka for the LAD of *P. lacunosa* and 268 Ka for the FAD of *E. huxleyi*; i.e., slightly above ours (Fig. 2).

Unfortunately there is no available oxygen isotope record for the interval between 329 and 560 Ka and thus nannofossil stratigraphy and paleomagnetism are the only tools to obtain additional datum levels of chronological significance. The nannofossil LAD of *P. lacunosa* at 458 Ka dated by Thierstein et al. (1977) and the paleomagnetic event dated in 780 Ka by Mix et al. (2003) at Site 1240, were the reference points used for that period (Table 1). The age model was obtained by linear interpolation between these reference points using the "Analyseries" software of Paillard et al. (1996). It is possible that the age model for Site 1240 can be slightly improved in the future when the oxygen isotope stratigraphy is extended back in time.

Table 1
Control points used to develop the age mode

Control points	Depth (mcd)	Age (Ka)	Authors
δ^{18}O: *G. ruber* white	0.01	2	Cacho et al., in prep.
δ^{18}O: *G. ruber* white	2.33	17	Cacho et al., in prep.
δ^{18}O: *G. ruber* white	10.07	65	Cacho et al., in prep.
δ^{18}O: *G. ruber* white	14.05	122	Cacho et al., in prep.
δ^{18}O: *G. ruber* white	14.97	132	Cacho et al., in prep.
δ^{18}O: *G. ruber* white	18.07	164	Cacho et al., in prep.
δ^{18}O: *G. ruber* white	27.14	245	Cacho et al., in prep.
δ^{18}O: *G. ruber* white	30.23	286	Cacho et al., in prep.
δ^{18}O: *G. ruber* white	33.00	329	Cacho et al., in prep.
Biostratigraphic datum: LAD *P. lacunosa*	43.66	458	Flores et al., 2006
Paleomagnetic datum	70.00	780	Mix et al., 2003

3.3. Estimation of abundances, nannofossil accumulation rate (NAR) and coccolith $CaCO_3$ contribution

Absolute coccolith abundances (nannofossils g^{-1}) and the NAR were calculated using the formula given by Flores and Sierro (1997). The NAR (nannofossils cm^{-2} Ka^{-1}) was calculated using estimations of the number of coccoliths per gram (coccolith g^{-1}), GRAPE densities (d, g cm^3), obtained by Mix et al. (2003), and the linear sedimentation rate (SR, cm Ka^{-1}), derived from the age model. GRAPE densities were used since dry sediment densities were not available.

The contribution of coccoliths to the overall carbonate flux (Mass, pg g^{-1}) was assessed using the method proposed by Young and Ziveri (2000), using the species-specific mean coccolith length (μm^3), absolute abundances in the sediment (nannofossils g^{-1}), the shape factor (k_s) for each species and the calcite density (2.7 pg μm^{-3}). Table 2 summarises the source of coccolith k_s values, mean coccolith length, and the coccolith carbonate content for each species. This method allows the estimation of coccolith-derived $CaCO_3$ from individual species, although a significant cumulative error (around 50%) is involved (Young and Ziveri, 2000). A key potential source of errors is variation in size of individual species between samples. Also, broken coccoliths were not taken into account (although they do not appear to be significant), and hence the coccolith carbonate contribution could be higher than computed. So, the calculations of the coccolith carbonate content should be interpreted with caution.

The *N* ratio paleoproductivity proxy was proposed by Flores et al. (2000) based on the relative abundance of the main surface eutrophic species (small Noelaerhabdaceae, R) and the main lower photic zone species (*Florisphaera profunda*, F). Thus, high values indicate strong upwelling and shallow stratification (values closer to 1) while low values indicate weak upwelling and deep stratification (values closer to 0). In this work, this function was modified to include *Gephyrocapsa oceanica* (Go), a species that was absent from the original function. *G. oceanica* is one of the most abundant surface species in the core and has mainly been reported in surface waters in tropical and subtropical areas (Okada and Honjo, 1973; Okada and McIntyre, 1979; Beaufort and Buchet, 2003), in upwelling areas of low latitudes: the Panama Basin (Giraudeau et al., 1993; Hagino and Okada, 2004; Martínez et al., 2005), northwest Africa (Geitzenauer et al., 1977), the Red Sea (Winter, 1982) and monsoon-induced upwelling waters (Houghton and Guptha, 1991), and it has also been described in the relatively warm upwelling waters of the Beguela area (Giraudeau, 1992). Accordingly, the modified *N* ratio proposed and used in this core is:

$$N = \frac{R + \mathrm{Go}}{R + \mathrm{Go} + F}.$$

3.4. Taxonomic notes

The most abundant group of taxa at the site belong to the family Noelaerhabdaceae, including *Gephyrocapsa oceanica*, *G. muellerae*, *G. caribbeanica*, *E. huxleyi*, small *Reticulofenestra* and *P. lacunosa*. The morphotaxonomy used for the genus *Gephyrocapsa* was adopted from Flores et al. (2000) and is summarised in Table 3. Small placoliths <3 μm long with an open central area and small placoliths <2.5 μm long with a closed central area were grouped as small Noelaerhabdaceae, this includes small *Gephyrocapsa* (*G. aperta* and *G. ericsonii*), small *Reticulofenestra*, and rare *E. huxleyi*. Other small placoliths between 2.5 and 3 μm but with a closed central area were included in the small Noelaerhabdaceae as a small morphotype of *G. caribbeanica*. This difference in the small Noelaerhabdaceae was considered for coccolith carbonate calculations. Different sizes of *G. oceanica* were also considered for carbonate calculations (medium *Gephyrocapsa* 3–4 μm and large *Gephyrocapsa* 4–5 μm), but later these sizes were lumped as *G. oceanica* for paleoecological purposes. *Calcidiscus leptoporus* and *Helicosphaera carteri* are subordinate species and were present throughout the record. Although *Coccolithus pelagicus*, a subordinate species, was very rare and sporadic, it was considered for coccolith carbonate estimations. The group of species categorised as warm and oligotrophic taxa include *Umbilicosphaera sibogae*, *Calciosolenia murrayi*, *Neosphaera coccolithomorpha*, *Oolithotus* spp., *Pontosphaera* spp., *Rhabdosphaera clavigera*, *Syracosphaera* spp. and *Umbellosphaera* spp. (Boeckel and Baumann, 2004) and were lumped together. *Umbilicosphaera*, a major component of the warm taxa, includes three species: *U. sibogae*, *U. foliosa* and *U. hulburtiana*. These species were counted separately but were grouped together because they did not show a paleoecologically different behaviour. Also, species of the genera *Oolithotus*, *Pontosphaera*, *Syracosphaera* and *Umbellosphaera* were not distinguished by Light Microscope and were counted together in their corresponding genus.

4. Results

4.1. Calcareous nannofossil assemblages and the N ratio

Small Noelaerhabdaceae, *G. oceanica* and *F. profunda* were the most abundant species throughout the interval studied, although *F. profunda* was only abundant during MIS 5 (Fig. 4a and b; Plates I and II). Small Noelaerhabdaceae constitute between ~50% and ~11% of the total assemblage. In some intervals, the small Noelaerhabdaceae appeared alternately with *G. oceanica*. The relative abundances of *G. oceanica* increased up-core reaching maximum abundances of 60%. *F. profunda* abundances increased slightly from MIS 8 (less than 10%) to MIS 6 and then abruptly in MIS 5e, when this species reached ~62%. Major changes in the composition and

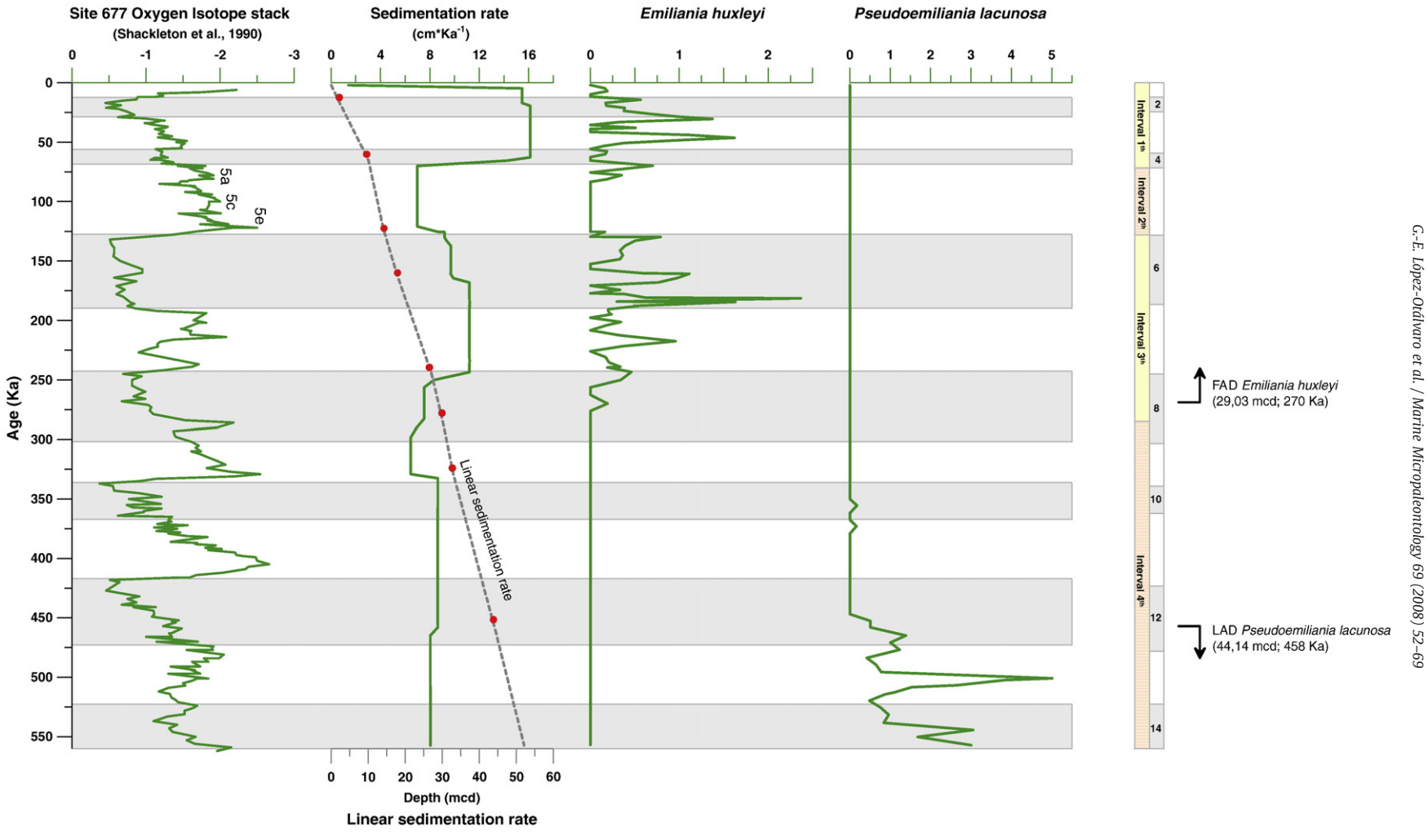

Fig. 2. Oxygen Isotope Stack from Site 677, compared to sedimentation rates and biostratigraphic events identified at ODP Site 1240: FAD (First Appearance Datum) of *Emiliania huxleyi* and LAD (Last Appearance Datum) of *Pseudoemiliania lacunosa*, (Table 2). Grey bars indicate glacial isotope stages 2 through 14. 5a, 5c, 5e: substages of MIS 5. Small circles in linear sedimentation rates indicate control points.

Table 2
Summary of coccolith shape constants used (k_s) and carbonate coccolith estimations for each species (mean length) at ODP Site 1240

Species	k_s	k_s source	Mean length	Vol at mean length (μm)^3	Coccolith $CaCO_3$ at mean length (pg)
Calcidiscus leptoporus	0.080	Young and Ziveri (2000)	7.0	27.440	74.088
Emiliania huxleyi	0.020	Young and Ziveri (2000)	2.5	0.313	0.844
Florisphaera profunda	0.040	Young and Ziveri (2000)	3.3	1.437	3.881
Gephyrocapsa caribbeanica	0.060	Adopted from *G. oceanica*'s k_s maximum value	3.0	1.620	4.374
Small Noelaerhabdaceae (*G. ericsonii* and *G. aperta*)	0.050	Adopted from *G. ericsonii*	2.0	0.400	1.080
Gephyrocapsa muellerae	0.050	Young and Ziveri (2000)	3.0	1.350	3.645
Gephyrocapsa oceanica	0.050	Young and Ziveri (2000)	3.5	2.144	5.788
Large *Gephyrocapsa*	0.050	Adopted from *G. oceanica*	4.5	4.556	12.302
Helicosphaera carteri	0.050	Young and Ziveri (2000)	10.0	50.000	135.000
Pseudoemiliania lacunosa	0.040	Adopted from *E. huxleyi* type A normally calcified	4.5	3.645	9.842
Warm taxa					
Calciosolenia murrayi	0.030	Young and Ziveri (2000)	3.5	1.286	3.473
Neosphaera coccolithomorpha	0.015	Young and Ziveri (2000)	6.5	4.119	11.122
Oolithotus cavum	0.070	Adopted from *O. cavum*	4.0	4.480	12.096
Oolithotus fragilis	0.070	Young and Ziveri (2000)	5.0	8.750	23.625
Pontosphaera spp.	0.050	Adopted from *H. carteri* (Zygodiscales)	8.0	25.600	69.120
Rhabdosphaera clavigera	0.025	Young and Ziveri (2000)	8.0	12.800	34.560
Syracosphaera spp.	0.030	Adopted from *S. pulchra*	4.0	1.920	5.184
Umbellosphaera spp.	0.010	Young and Ziveri (2000)	4.0	0.640	1.728
Umbillicosphaera sibogae foliosa	0.060	Young and Ziveri (2000)	4.0	3.840	10.368
Umbillicosphaera sibogae hulburtiana	0.050	Adopted from *U. sibogae sibogae*	3.5	2.144	5.788
Umbillicosphaera sibogae	0.050	Young and Ziveri (2000)	4.0	3.200	8.640

absolute abundance of the assemblage, the NAR and coccolith-derived $CaCO_3$ were observed during the mid-Brunhes event between MIS 14-8 and during the warm MIS 5 (Fig. 3).

Another significant species is the heavily calcified *G. caribbeanica*, which was very abundant (up to 65%) during the mid-Brunhes event (MIS 14-8), and sometimes also alternated in abundance with the small Noelaerhabdaceae. The highest concentration of nannofossils is observed during MIS 14 to the early phase of MIS 8, coinciding with the maximum abundances of *G. caribbeanica* and its small morphotype. A marked reduction in the absolute abundances of coccoliths from the middle of MIS 8 to the Holocene was coincided with more prominent fluctuations of *F. profunda*.

C. leptoporus, *H. carteri* and the warm taxa, have combined abundances below 10%, throughout the studied interval. However, their contribution is significant in terms of carbonate production because they produced large, heavily calcified coccoliths. *H. carteri* and *C. leptoporus* reached their maximum abundances during MIS 6 and MIS 3. *G. muellerae* and the warm taxa, although subsidiary in the coccolithophore assemblage, displayed opposite short-term behaviour, but fairly similar long-term patterns. Thus, both *G. muellerae* and the warm taxa show increases in abundance during MIS 6 and especially MIS 4-1, but within these intervals they show anti-covariant patterns of peaks and troughs in abundance (Fig. 4a). Other species were recorded in very low abundances. In regard to coccolith preservation, Light and Scanning Electron Microscope observations revealed good to moderate preservation along the whole sequence studied.

The *N* ratio (Fig. 3) exhibits important variations of the interval studied. The highest and most uniform *N* ratio values were observed from MIS 14 to the beginning of MIS 8, coinciding with the maximum fluxes of coccoliths and their maximum carbonate production. This index gradually starts to decrease during MIS 8, showing fluctuations corresponding to peaks of *F. profunda*. The *N* values fall dramatically in isotope substage 5e, followed by an increase to pre-5e levels, which is interrupted by negative excursions in the substages 5c to 5a. Relatively high values are reached from MIS 4 to the Holocene. A general decreasing trend in *N* values over the last 560 Ka is evident and does not seem to be correlated with the glacial/interglacial pattern of variation in this system.

Table 3
Taxonomic notes and morphological differences used for the genus *Gephyrocapsa* (mainly adopted from Flores et al., 2000) in this study

This study	Small *Gephyrocapsa* (it includes *G. ericsonii*/*G. aperta*	Small morphotype of *G. caribbeanica*)	*G. muellerae* (it includes *G. margereli*)	*G. caribbeanica*	*G. oceanica*
Coccolith length	<3 μm	<2.5 μm	>3 μm	>2.5 μm	3 μm–5.5 μm
Bridge angle		Central area closed	5°–40°	Central area closed	>50°
Author equivalence					
Thierstein et al., 1977			*G. caribbeanica*		
Raffi et al., 1993	Small *Gephyrocapsa*		Small *Gephyrocapsa*	Small *Gephyrocapsa*	Medium *Gephyrocapsa*
Bollmann, 1997	*G.* minute		*G.* cold	*G. oligotrophic*, *G. transitional*	*G.* large, *G. equatorial*
Flores et al., 2000	Small *Gephyrocapsa*		*G. muellerae*	*G. caribbeanica*	*G. oceanica*
Baumann and Freitag, 2004	*G. ericsonii*/*G. aperta*		*G. muellerae*/*G. margereli*	*G. caribbeanica*	*G. oceanica*

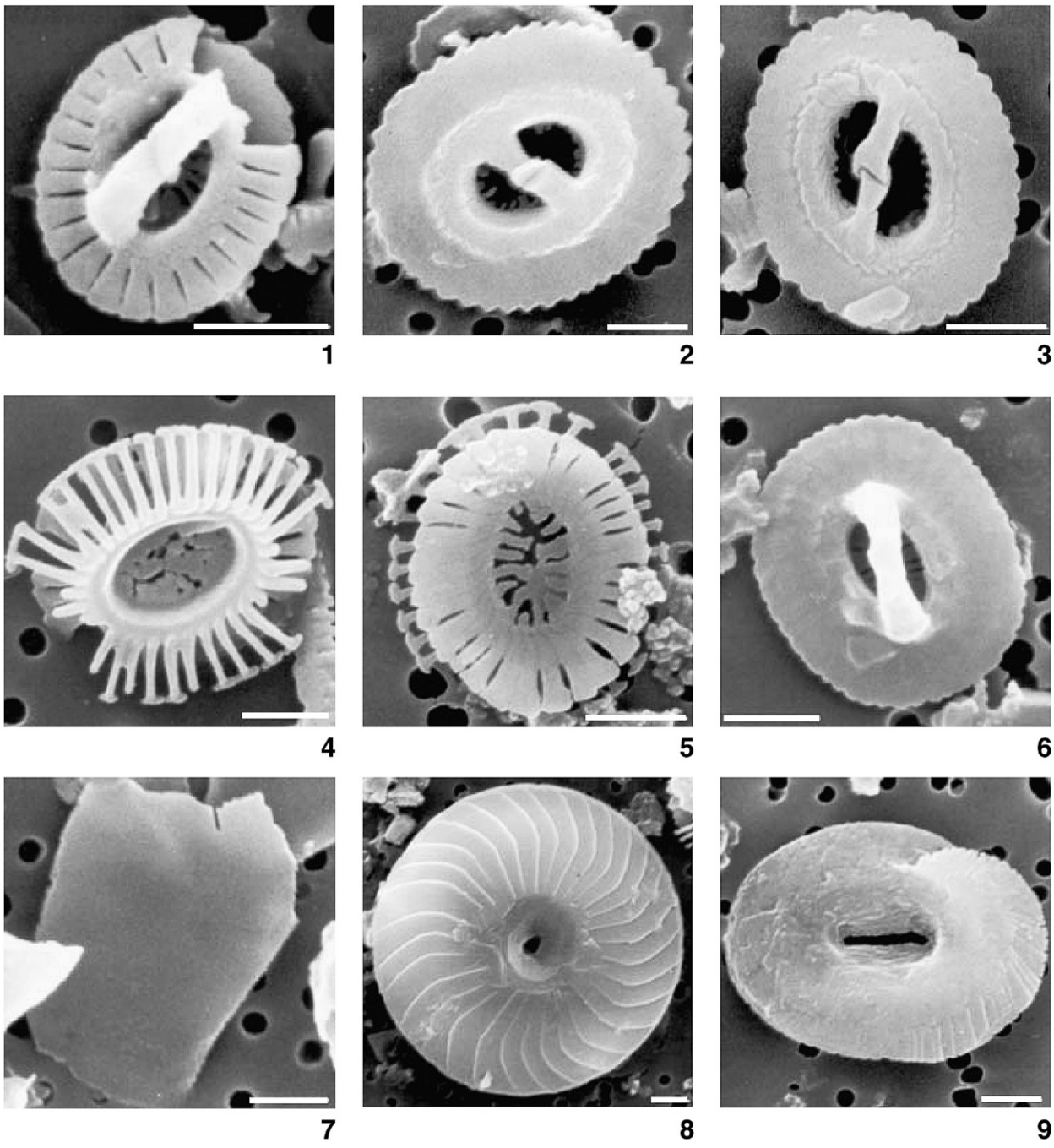

Plate I. SEM micrographs were taken at ODP Site 1240 in the Institute of Geosciences (CAU Kiel). Scale bars: 1 μm. 1. *Gephyrocapsa ericsonii* (mcd 19.97). 2. *Gephyrocapsa oceanica* (mcd 13.97). 3. *Gephyrocapsa muellerae* (mcd 41.13). 4. *Emiliania huxleyi* (mcd 12.48). 5. *Emiliania huxleyi* (mcd 1.53). 6. *Gephyrocapsa* cf. *caribbeanica*, mcd 12.48. 7. *Florisphaera profunda* (13.97). 8. *Calcidiscus leptoporus* (mcd 5.34). 9. *Helicosphaera carteri* (mcd 13.97).

4.2. Sedimentation and nannofossil accumulation rates

The site is characterised by high average sedimentation rates (9.3 cm Ka^{-1}) (Fig. 2), maximum values being observed during MIS 4-1. By contrast, the lowest sedimentation rates occur during MIS 9-8 and MIS 5 (~7 cm/Ka). The low sedimentation rates during MIS 14-10 may be an artefact of the few reference points used in the age model for this interval (Fig. 2).

The total accumulation rates of calcareous nannofossils at Site 1240 are high over the last 560-Ka (Fig. 3), around 5×10^{10} to 4×10^{11} nannofossils cm^{-2} Ka^{-1}, and decrease upwards. Our study reveals that the major contributors to the nannofossil accumulation rates (NAR) were *G. caribbeanica*, the small

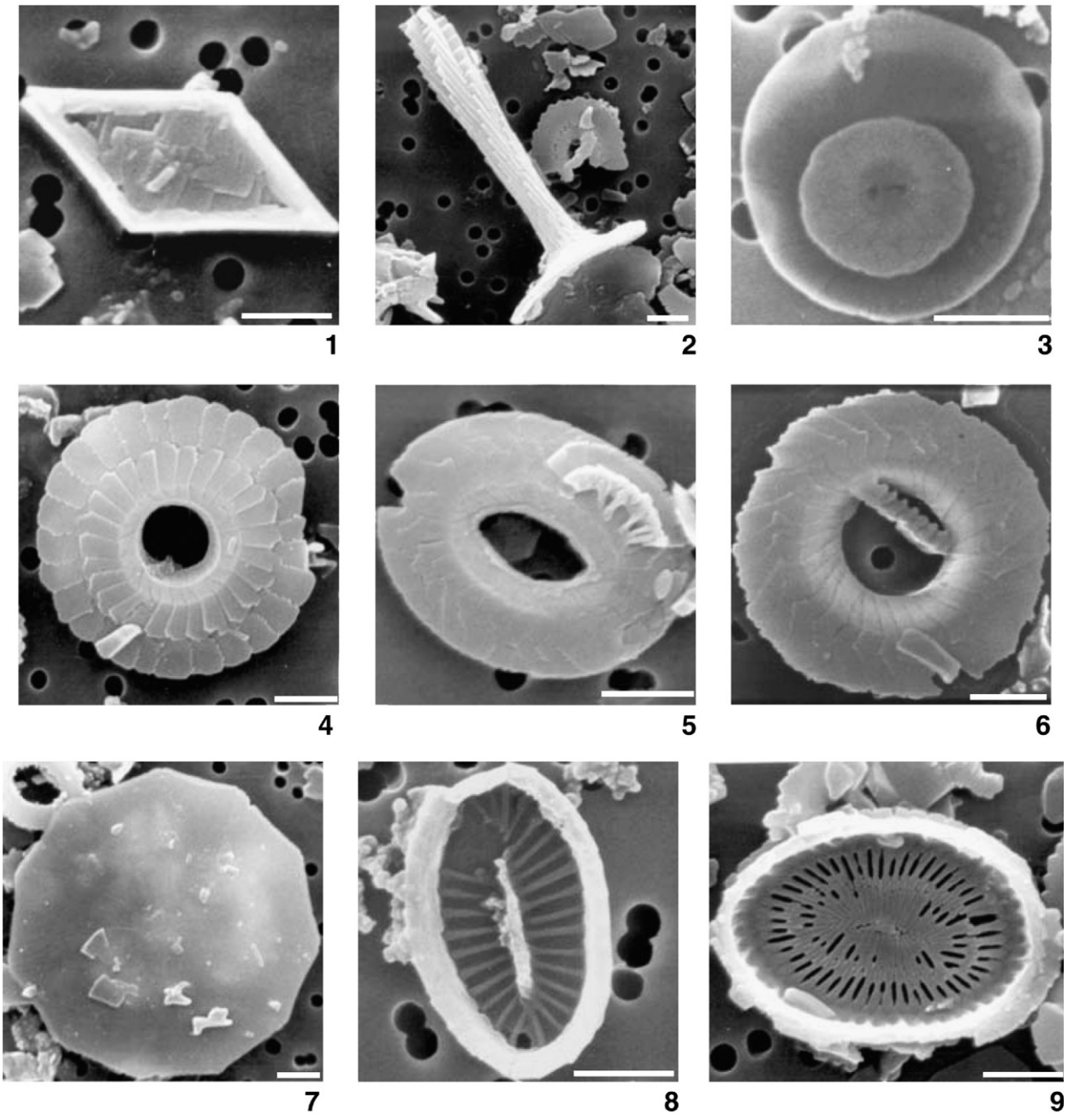

Plate II. SEM micrographs were taken at ODP Site 1240 in the Institute of Geosciences (CAU Kiel). Scale bars: 1 μm. 1. *Calciosolenia murrayi* (mcd 19.97). 2. *Rhabdosphaera clavigera* (mcd 41.68). 3. *Oolithotus antillarum* (mcd 1.53). 4. *Umbilicosphaera. foliosa* (mcd 41.68). 5. *Umbilicosphaera hulburtiana* (mcd 8.12). 6. *Umbilicosphaera sibogae* (mcd 12.48). 7. *Hayaster perplexus* (mcd 41.68). 8. *Syracosphaera lamina* (mcd 1.53). 9. *Syracosphaera pulchra* (mcd 41.68).

Noelaerhabdaceae and *G. oceanica* (Fig. 4a and b), and their fluxes alternated reciprocally. A lower NAR coincides with the fall in the abundances of *G. caribbeanica*. The lowest nannofossil accumulation rates occurred during MIS 5, coinciding with the dominance and maximum concentration of *F. profunda* in the assemblage. In spite of the high accumulation rates of the subordinate and highly calcified species *C. leptoporus*, *H. carteri* and *U. sibogae* during MIS 6, the total NAR was low during that time.

4.3. Coccolith carbonate mass

The contribution of coccolith-derived $CaCO_3$ varies considerably and followed a prominent pattern along the mid-Brunhes event, coinciding with the *G. caribbeanica* extra component of the assemblage (Figs. 3 and 4b). The highest values are found during MIS 14-8 (Figs. 3, 5a and b). In spite of their low abundances, the major contributors to the coccolith carbonate are the heavily calcified species *G. caribbeanica* (up

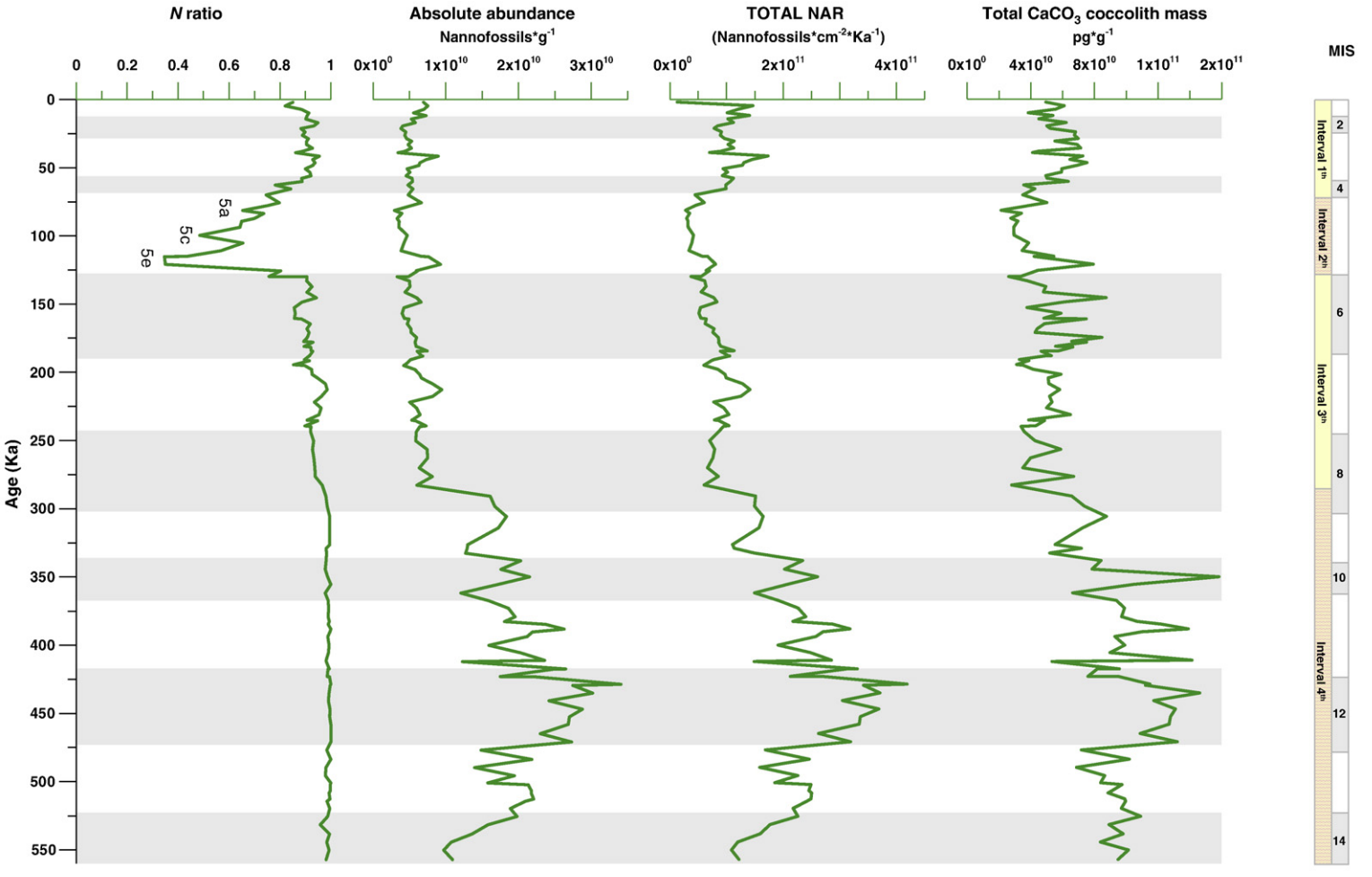

Fig. 3. Review of the major bioproductivity proxies at Site 1240: *N* ratio (proportion of *F. profunda* to small Noelaerhabdaceae and *G. oceanica*) vs. total absolute abundance of coccoliths, their accumulation rate (NAR) and the calculated total mass of coccolith $CaCO_3$ per gram of sediment (NB 1 g = 10^{12} pg). Grey bars indicate glacial isotope stages 1 through 14. 5a, 5c, 5e: substages of MIS 5. The paleoceanographic intervals discussed in Section 5 are included.

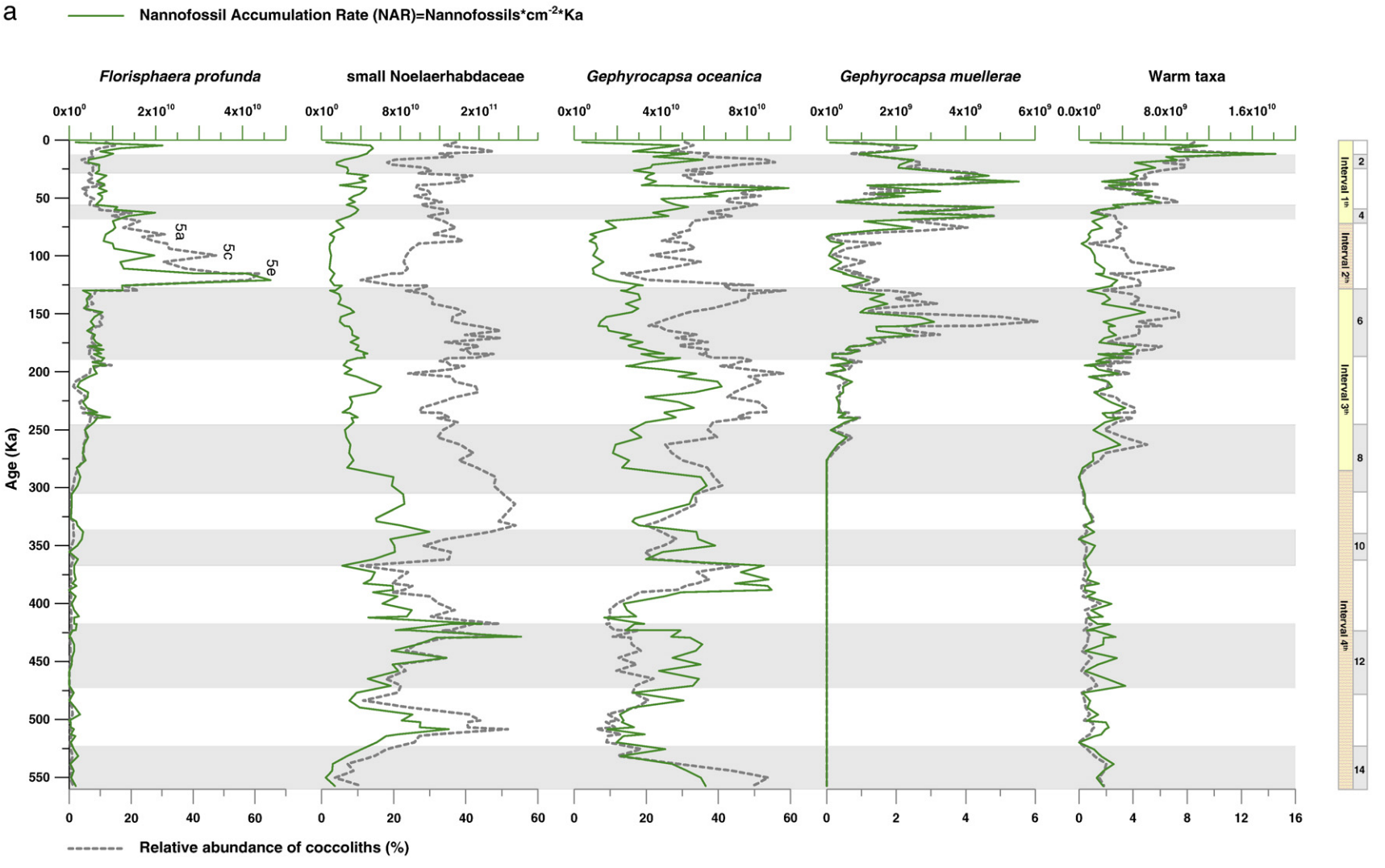

Fig. 4. a. Relative abundances (%) and accumulation rates of the most significant nannofossil species. Grey bars indicate glacial isotope stages 2 through 14. 5a, 5c, 5e: substages of MIS 5. The paleoceanographic intervals discussed in Section 5 are included. b. Relative abundances (%) and accumulation rates of heavily calcified species. Grey bars indicate glacial isotope stages 2 through 14. The paleoceanographic intervals discussed in Section 5 are included.

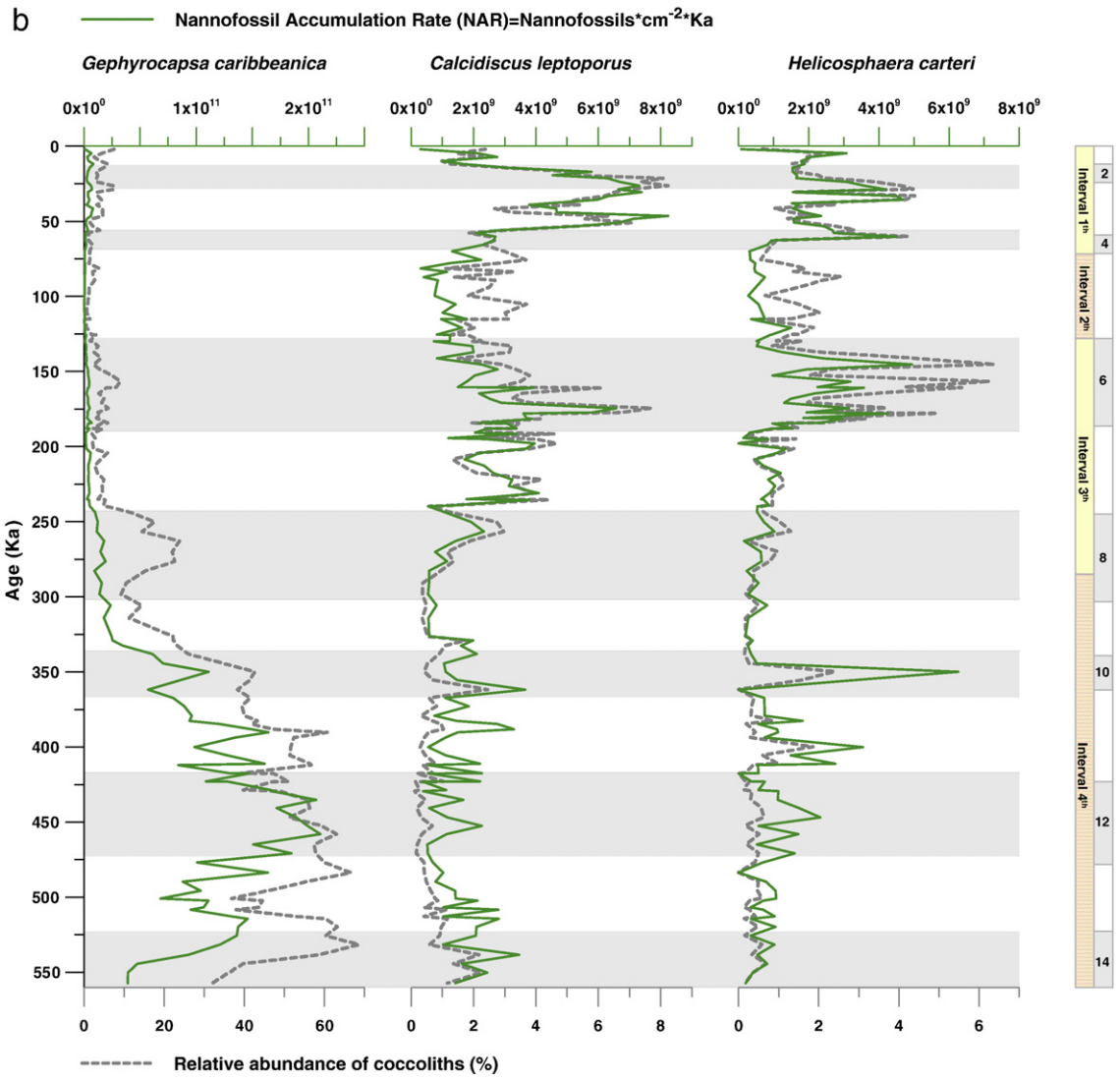

Fig. 4 (*continued*).

to ~65%), *H. carteri* (up to ~60%) and *C. leptoporus* (up to ~50%). Other very important calcite producers are *G. oceanica*, with a relative production of up to ~50%, and the small Noelaerhabdaceae (up to ~16%) owing to their high abundances in the assemblage (Fig. 5a and b). The carbonate contribution during MIS 5e is dominated by *F. profunda*.

5. Discussion

Coccolithophores strongly contributed to the paleoproductivity and to the accumulation of the sediments along the last 560 Ka at ODP Site 1240. Many authors have used nannofossils, especially upper photic zone dwellers such as small Noelaerhabdaceae, (Young, 1994; Okada and Wells, 1997; Wells and Okada, 1997; Flores et al., 1999, 2000, 2003; Bollman et al., 1998; Beaufort et al., 1999; Beaufort and Buchet, 2003) and *G. oceanica* (see Section 3.3), as paleoproductivity proxies in upwelling areas (Young, 1994; Baumann and Freitag, 2004) and in equatorial high-productivity locations (Hagelberg et al., 1995; Weber, 1998). *F. profunda* normally grows at a depth close to the nutri-thermocline when the water column is stratified (Okada and Honjo, 1973; Molfino and McIntyre, 1990a,b; Young, 1994; Okada and Wells, 1997; Wells and Okada, 1997; Beaufort et al., 1997, 1999, 2001, 2003; Beaufort and Buchet, 2003; Flores et al., 2000; Liu and Herbert, 2004; Baumann and Freitag, 2004). This species has also been considered as a sea water transparency indicator (Ahagon et al., 1993).

Variations in the assemblage over the last 560 Ka are related to changes in the dynamics of the water column that regulate nutrient content and sea surface temperature: hence the dominance of the nannofossil species near the equator. An ecological alternation could explain the alternating dominance of small Noelaerhabdaceae (related to maximum eutrophication) and *G. oceanica* (associated with highly eutrophic and moderately warm sea surface waters) in response to slight sea

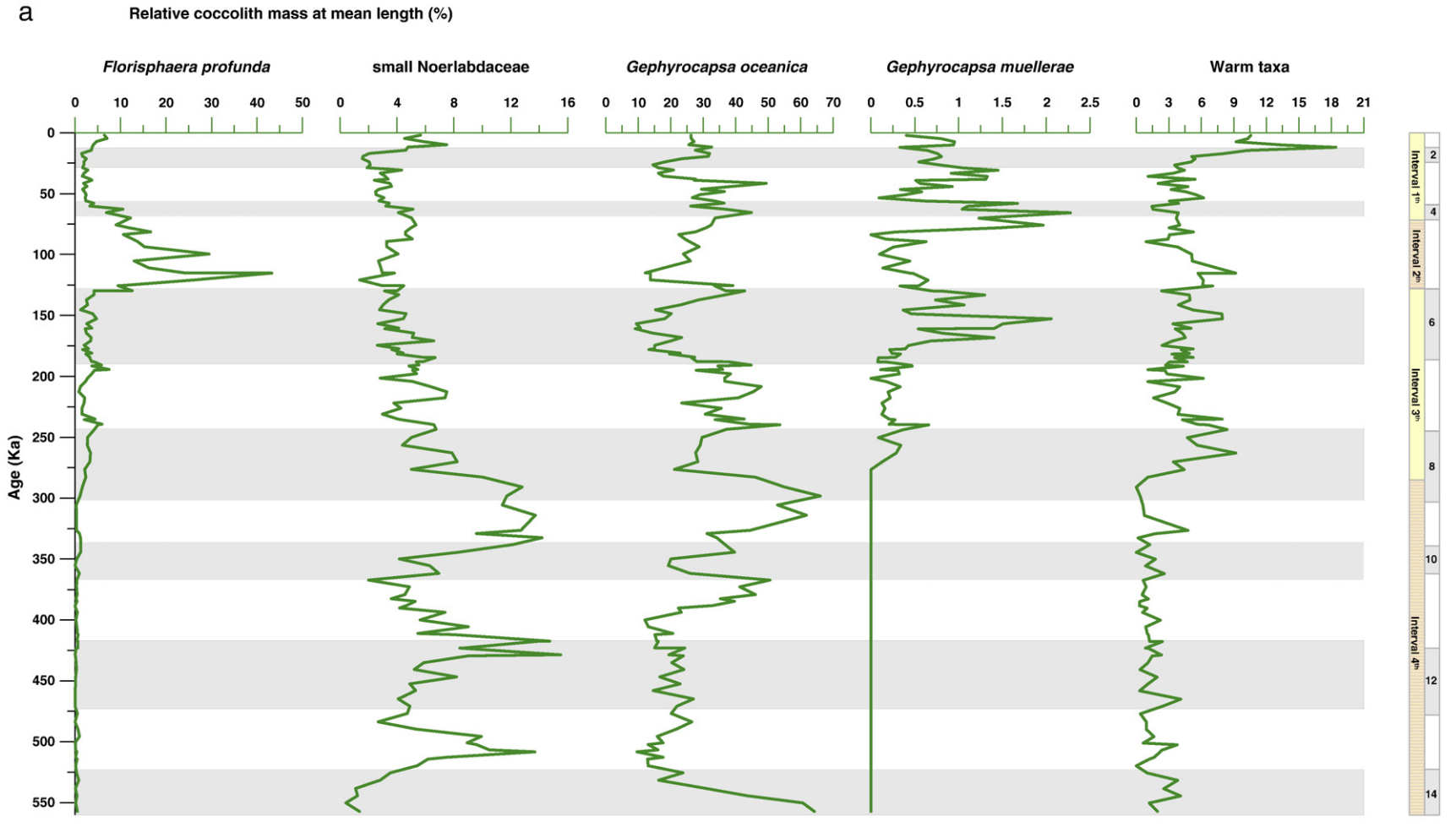

Fig. 5. a. Coccolith carbonate contributed by the most abundant coccolithophores at Site 1240. Grey bars indicate glacial isotope stages 2 through 14. The paleoceanographic intervals discussed in Section 5 are included. b. Coccolith carbonate contributed by heavily calcified coccolithophores at Site 1240. Grey bars indicate interglacial isotope stages 2 through 14. The paleoceanographic intervals discussed in Section 5 are included.

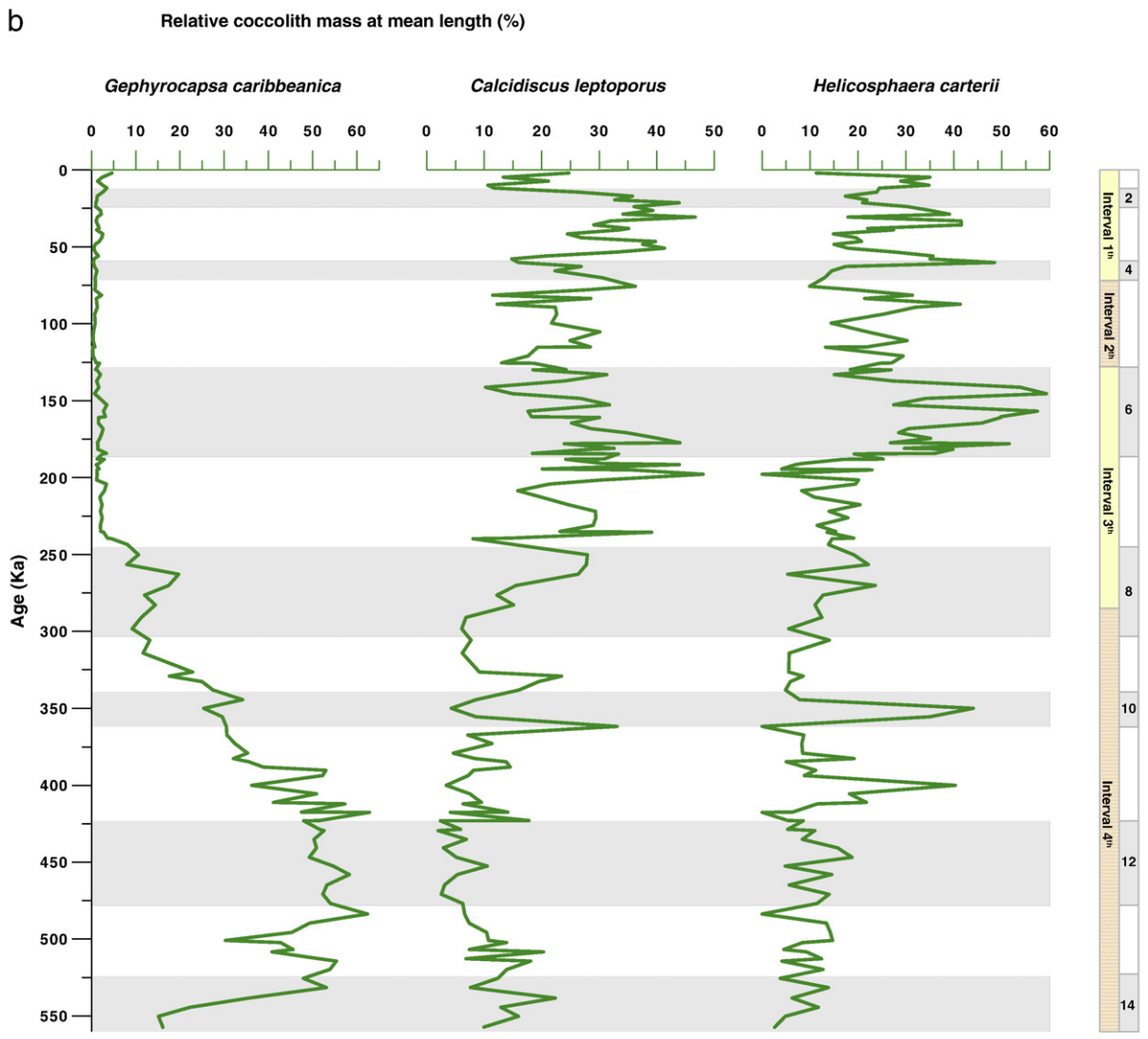

Fig. 5 (*continued*).

surface temperature changes, as proposed by Hagino and Okada (2004) for the Equatorial Pacific.

It is possible that the low abundance of *C. pelagicus* and *E. huxleyi* at this site was mainly temperature-induced. *C. pelagicus* has been reported as an inhabitant of low-temperature upwelling waters (Cachao and Moita, 2000). Okada and Honjo (1975), Houghton and Guptha (1991) linked the scarcity of *E. huxleyi* to the higher concentration of *G. oceanica* in the nutrient-rich waters of the open tropical and subtropical regions of the Red Sea and the Western Pacific.

The variability of the NAR and coccolith $CaCO_3$ contents was used here as proxies for bioproductivity, the calcified nannofossils being the main suppliers of calcium carbonate to the sediments. Coccoliths are considered to be the main component of the sediment during the interval studied (Mix et al., 2003) and hence should be the major contributor to total carbonate for the last 560 Ka. Unfortunately, carbonate analyses are not available and it is therefore not possible to assess the contribution of coccoliths to the total carbonate in the sediments. Assemblage fluctuations provide an important source of information about paleoproductivity and carbonate coccolith data.

Based on this analysis, a continuous record of coccolithophore paleoproductivity was elaborated using the *N* function. Significant changes in this function allowed us to distinguish four paleoceanographic intervals over the last 560 ka (Fig. 3).

5.1. Interval 1: MIS 14-8: ~283 Ka to ~560 Ka (~29.99 mcd to ~52.10 mcd)

This interval, characterised by coccolith-rich material has very high *N* values, the consequence of high fertility in surface waters, which was probably associated with strong upwelling and high bioproduction. The abundance of the small Noelaerhabdaceae and *G. oceanica* would correspond to a well defined Equatorial Cold Tongue in the EEP, caused by a

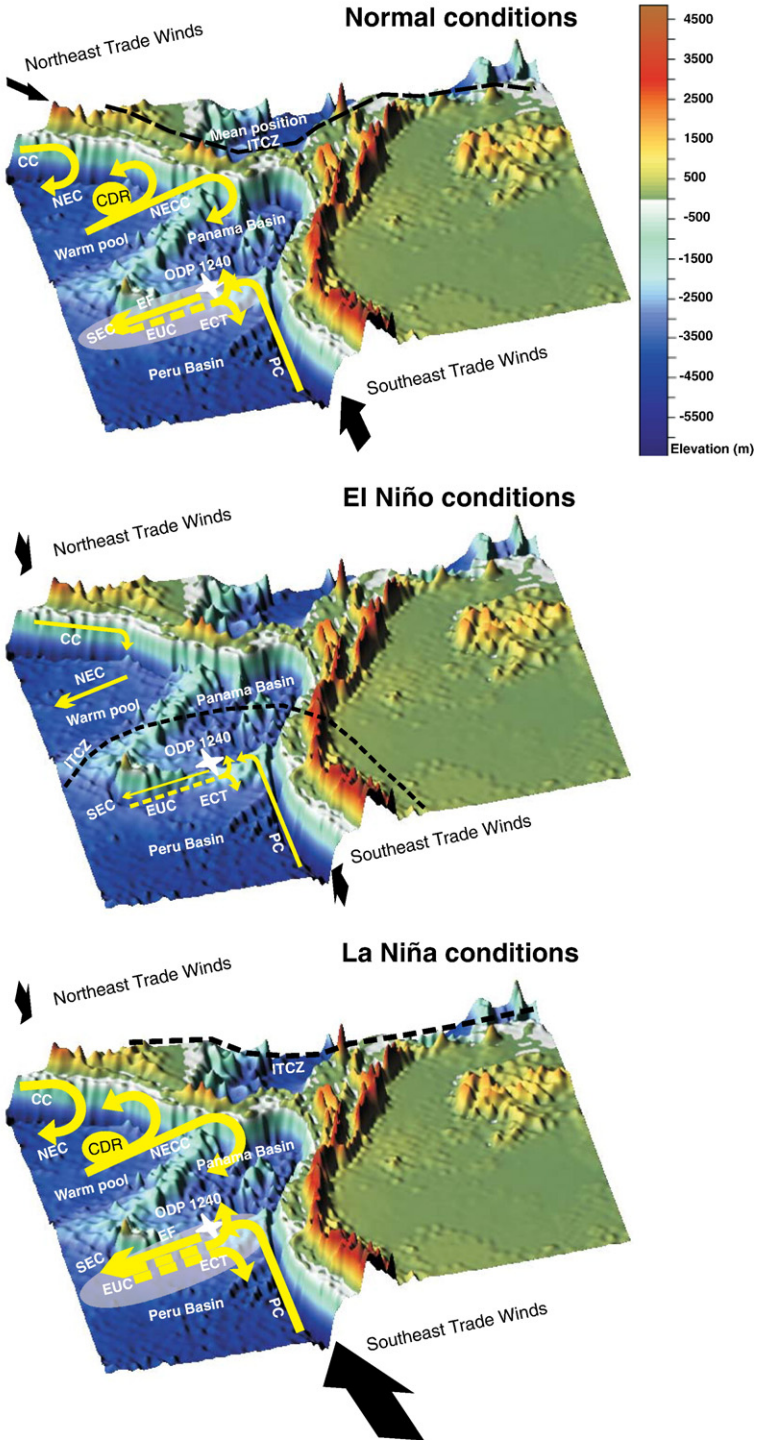

Fig. 6. Atmospheric and oceanic conditions during periods of normal, El Niño-like and La Niña-like conditions. PC: Peru Current, SEC: South Equatorial Current, EUC: Equatorial Undercurrent, NEC: North Equatorial Current, CC: California Current, NECC: North Equatorial Counter Current, CDR: Costa Rica Dome, ECT: Equatorial Cold Tongue, (Normal conditions adapted from Fiedler and Talley, 2006; and Kessler, 2006). ITCZ: Intertropical Convergence Zone (Mean position of the ITCZ adapted from Philander, 1995). Colour scale highlighting major bathymetric features (taken from topography database from Smith and Sandwell (1997)).

shallow nutri-thermocline through the reinforcement of the EUC and the SEC, and the displacement of the ITCZ at its northernmost position due to the enhancement of the southeast trades, which favoured the proliferation of these species. The highest abundances of the upper photic zone inhabitants together with the highest NAR and the maximum concentration of coccolith carbonate (Fig. 4a) suggest intense upwelling episodes. These conditions were probably related to a period of higher frequency and more intense La Niña-like events (Fig. 6).

The co-occurrence of low magnetic susceptibility, high lightness values (L^*), and high $CaCO_3$ accumulation rates reported by Mix et al. (2003), supports the above interpretation. Jansen et al. (1986) reported the marked northward displacement of oceanic fronts, allowing the strengthening of the Southern Hemisphere circulation in all oceans between 300 and 400 Ka. Other studies have searched for a connection between primary productivity, the movement of the thermonutricline, wind stress and ENSO events in the equatorial Indopacific oceans (Beaufort et al., 1997, 2001).

The period from MIS 14-8 has been referred to as the mid-Brunhes event and corresponds to a global increase in the carbonate content of pelagic sediments (Droxler et al., 2003) and a significant increase in the global abundance of the heavily calcified *G. caribbeanica* (Bollmann et al., 1998, in the Atlantic, Southwestern Pacific and Southern oceans; and by Flores et al., 1999, 2003, Baumann and Freitag, 2004, and Baumann et al., 2004, at high latitudes). *G. caribbeanica* was excluded from the *N* ratio because it is almost absent in the upper intervals. Nevertheless, this upper photic species could be considered a proxy of high paleoproductivity. Thus, a superimposed global or evolutionary pattern can be ruled out.

Although carbonate dissolution was intensive during the mid-Brunhes event, good to moderate coccolithophore preservation is found for this period at Site 1240. This suggests that there was no vertical change in the water masses overlying the sediment, and hence the carbonate compensation depth (CCD) and the lysocline must have been deeper than 2900 m during even that event. The presence of a deep lysocline during this interval, when other areas of the Equatorial Pacific were subject to strong dissolution, could be the consequence of high local rates of carbonate supply to deep waters (Archer 1991a,b).

5.2. Interval 2: MIS 10-6: ~128 to ~283-Ka (14.77 mcd to ~29.99 mcd)

A slight long-term reduction in the *N* ratio starting 283 Ka ago suggests less intense upwelling conditions in surface waters. Likewise, the progressive increase in the warm-water taxa during the last 283 Ka seems to indicate that SSTs were probably due to variations in the depth of the nutri-thermocline. These records, together with the decreasing upward trends of the NAR and coccolith carbonate mass, were probably the result of a progressive reduction in Trade wind intensity. This is fairly consistent with the results obtained by Scharmm (1985) and Emeis et al. (1995), who suggested that the Southern Hemisphere circulation was reduced over the last 500 Ka, favouring the warming of surface waters in the EEP. At Site 1240, this warming is more apparent during the last 283 Ka.

The oceanographic situation during this interval may have been dominated by La Niña-like conditions, punctuated by short periods in which El Niño-like events were more frequent (Fig. 6). This interval could have been the prelude to an oceanographic scenario that developed fully during MIS 5, with similar oceanographic conditions to those existing today during El Niño events.

5.3. Interval 3: MIS 5: ~71-Ka to ~128-Ka (~10.82 mcd to ~14.77 mcd)

This interval, defined by an abrupt increase in *F. profunda* and so a decrease in *N* values (Figs. 3, 4a and b), is characterised by a remarkable change in the coccolith assemblage, suggesting that the water column of the EEP became more stratified, leading to a reduction in nutrient supply in surface waters and a deepening of the nutri-thermocline. All paleoproductivity proxies (*N* ratio, NAR, and coccolith carbonate) seem to indicate a collapse in the upwelling system (Fig. 3). The sediments may have been slightly affected by dissolution, resulting in a weak relative increase in *F. profunda*, although the presence of small Noelaerhabdaceae, the low abundances of *G. oceanica* and the identification of all coccoliths at species level suggest that dissolution, if it occurred, would have been moderate.

Evidence from other proxies, such as high magnetic susceptibility values (Mix et al., 2003), suggests reduced atmospheric circulation in the EEP, since low wind intensities favour the settling of the finest eolian magnetic particles (Hovan, 1995). A low $CaCO_3$ content for the last interglacial period (MIS 5) has been reported previously by Lyle et al. (1988), Lyle et al. (2002), Thomas et al. (2000), Snoeckx and Rea (1994) and Murray et al. (1995) for the Eastern Tropical Pacific, suggesting low carbonate sedimentation due to low carbonate productivity at that time (Hagelberg et al., 1995). Other proxies, such as planktonic foraminifer Mg/Ca values, indicate the presence of very warm SSTs during MIS 5e (Lea et al., 2006), in agreement with the low *N* values and the strongly stratified water column found in this work. Beaufort and Buchet (2003) reported a relationship between the increases in *F. profunda* and the El Niño-like warm pool in the Western Pacific. Warmer conditions during El Niño-like events were linked to lower primary productivity during MIS 5 in the Indian and Pacific equatorial oceans (Beaufort et al., 1997, 2001).

The above evidence suggests a deepening of the nutri-thermocline and the arrival of the warm pool at Site 1240, in response to a weakening of the southeast trades during MIS 5e (Fig. 6), mostly associated with El Niño-like conditions with some fluctuations.

5.4. Interval 4: MIS 4-1: Holocene to ~71-Ka (0.03 mcd to ~10.82 mcd)

The *N* values (Fig. 3) during this interval as well as the accumulation rate of coccoliths and coccolith-derived carbonate were higher during MIS 4-1 than during the anomalous MIS 5. This situation is typically related to intense eutrophic conditions, also associated with enhanced biogenic opal production. Intensification of the southeast trades, together with a northward displacement of the ITCZ, would have driven the Equatorial Cold Tongue to the equator, resulting in high nutrient supply to the surface waters (Fig. 6). Atmospheric and oceanographic conditions were comparable to those

observed under the influence of La Niña-like events (Fig. 6). The *N* ratio seems to have reversed during the Holocene, indicating a slight decline in paleoproductivity, but it is still very high and therefore consistent with the results reported by Ravelo and Shackleton (1995), Farrell et al. (1995) and Rickaby and Halloran (2005), who suggested a shallower thermocline during the Holocene. Moreover, the increase in the frequency of fluctuations in the *N* ratio suggests that El Niño-like events were more frequent.

6. Conclusions

Our results suggest that the long-term variation in the nannofossil record for Site 1240 is an important tool for investigating the variability of the EEP and its response to paleoceanographic and paleoatmospheric conditions over the last seven glacial/interglacial cycles. In particular, the nannofossil assemblage, the nannofossil accumulation rate, and coccolith-derived $CaCO_3$ provide detailed historical information about surface water paleoproductivity and the displacement of the nutri-thermocline, both due to variations in intensity of the Trade wind system.

The dominance of small Noelaerhabdaceae, *G. oceanica* and *G. caribbeanica* indicates that the presence of nutrient-rich waters is indeed characteristic of high productivity in the upper photic zone, due to a shallow nutri-thermocline. These species imply the influence of the cool and subpolar waters and stronger Trade winds. The dominance of *F. profunda* is linked to a reduction in the intensity of the southeast Trade winds, a weakening of the upwelling, and the arrival of the warm pool at Site 1240. Likewise, small Noelaerhabdaceae and *G. oceanica* show an ecological alternance between high nutrient availability and cool temperatures in the upper photic zone, followed by eutrophic and moderately warm sea surface temperatures. The long-term pattern of the warm taxa and *N* values may be related to a relative reduction in upwelling intensity and a warming trend at the sea surface over the last 560 Ka. On the other hand, the rare concentrations of *E. huxleyi* and *C. pelagicus* could be temperature-induced, whereas *C. leptoporus* and *H. carteri* do not appear to show any ecological preference.

The interval studied was divided into four parts characterised by different paleoceanographic/paleoatmospheric conditions as indicated by variations in the *N* index, nannofossil accumulation rates, and coccolith-derived $CaCO_3$. Higher *N* values occurred during Interval 1 (MIS 14-8) during the mid-Brunhes event, suggesting a shallow nutri-thermocline and enhanced upwelling. This situation corresponds to maximum NAR and coccolith carbonate, possibly related to La Niña-like events. Interval 2 (MIS 8-6) shows high *N* values, although with fluctuations, as a consequence of variations in the position of the nutri-thermocline. This scenario was associated with strong Trade winds and enhanced upwelling, possibly related to a La Niña-like dominant situation. Lower *N* values during Interval 3 (MIS 5) reveal a deep nutri-thermocline, due to a reduction in the southeast Trade wind stress and a reduction in the NAR and *N* index. This situation is interpreted as El Niño-like conditions. The water surface regime during Interval 4 (MIS 4-1) is marked by incursions of cold and nutrient-rich advected waters introduced by southeast Trade wind stress, which favoured the increase in the abundances of the upper photic species, the NAR and coccolith $CaCO_3$ contents, and the whole scenario can be interpreted as La Niña-like dominant period.

Acknowledgements

The authors wish to thank the ODP Program Leg 202 for providing samples for calcareous nannofossil analysis. Thanks are also given to Dr. Hanno Kinkel and Mrs. Ute Schuldt (Institute of Geosciences, CAU Kiel) for their support in the SEM lab and discussions. We are also very grateful to Drs. Jeremy Young, Sebastian Meier and two anonymous reviewers for their careful revision and contributions which highly improved this paper. Financial support from the Spanish Ministerio de Educación y Ciencia, through an FPI Fellowship (BES-2003-0010) provided to G.E. López-Otálvaro and from Spanish projects BTE2002-04670, REN2003-08642-C02/CLI and CGL2006-10593 from the Ministerio de Educación y Ciencia, and SA088/04 from the Consejería de Educación de la Junta de Castilla y León is acknowledged.

Appendix A. Taxonomic appendix

Calcidiscus leptoporus (Murray and Blackman, 1898) Loeblich and Tappan, 1978
Calciosolenia murrayi Gran, 1912
Coccolithus pelagicus (Wallich, 1877) Schiller, 1930
Emiliania huxleyi (Lohmann, 1902) Hay and Mohler in Hay et al., 1967
Florisphaera profunda Okada and Honjo, 1973
Gephyrocapsa aperta Kamptner, 1963
Gephyrocapsa ericsonii McIntyre and Bé, 1967
Gephyrocapsa caribbeanica Boudreaux and Hay, 1967
Gephyrocapsa muellerae Bréhéret, 1978
Gephyrocapsa oceanica Kamptner, 1943
Hayaster perplexus (Bramlette and Riedel 1954) Bukry 1973
Helicosphaera carteri (Wallich, 1877) Kamptner, 1954
Neosphaera coccolithomorpha Lecal-Schlauder, 1950
Oolithotus (Cohen, 1964) Reinhardt, in Cohen and Reinhardt, 1968
Oolithotus antillarum Reinhardt, in Cohen and Reinhardt, 1968
Pontosphaera Lohmann, 1902
Pseudoemiliania lacunosa (Kamptner 1963) Gartner 1969
Rhabdosphaera clavigera (Murray and Blackman, 1898)
Reticulofenestra Hay, Mohler and Wade 1966
Syracosphaera Lohmann, 1902
Syracosphaera lamina Lecal-Schlauder 1951
Syracosphaera pulchra Lohmann, 1902
Umbellosphaera Paasche, in Markali and Paasche, 1955
Umbilicosphaera hulburtiana Gaarder, 1970
Umbilicosphaera sibogae var. *foliosa* (Kamptner, 1963) Okada and McIntyre, 1977
Umbilicosphaera sibogae var. *sibogae* (Weber-van Bosse, 1901) Gaarder, 1970

References

Ahagon, N., Tananka, Y., Ujiié, H., 1993. *Florisphaera profunda*, a possible nannoplankton indicator of Late Quaternary changes in sea-water turbidity at the northwestern margin of the Pacific. Marine Micropaleontology 22, 255–273.

Archer, D.E., 1991a. Equatorial Pacific calcite preservation cycles: production or dissolution. Paleoceanography 6, 561–571.
Archer, D.E., 1991b. Modelling the calcite lysocline. Journal of Gephysical Research 96, 17037–17050.
Baumann, K.-H., Freitag, T., 2004. Pleistocene fluctuations in the northern Benguela current systems as revealed by coccolith assemblages. Marine Micropaleontology 52, 195–215.
Baumann, K.-H., Böckel, B., Frenz, M., 2004. Coccolith contribution to South Atlantic carbonate sedimentation. In: Thierstein, H.R., Young, J.R. (Eds.), Coccolithophores—from Molecular Processes to Global Impact. Springer-Verlag, Berlin-Heidelberg, pp. 367–402.
Beaufort, L., Buchet, N., 2003. Variability of specific coccolith $CaCO_3$ weight and primary production in the western Pacific warm pool during the last glacial cycle. Geophysical Research Abstracts (European Geosciences Union) 5, 13225.
Beaufort, L., Lancelot, Y., Camberlin, P., Cayre, O., Vincent, E., Bassinot, F., Labeyrie, L., 1997. Insolation cycles as a major control of equatorial Indian Ocean primary production. Science 278, 1451–1454.
Beaufort, L., Bassinot, F.C., Vincent, E., 1999. Primary production response to orbitally induced variations of the Southern Oscillation in the Equatorial Indian Ocean. In: Abrantes, F., Mix, A.C. (Eds.), Reconstructing Ocean History: a Window into the Future. Kluwer Academic/Plenum, New York, pp. 245–272.
Beaufort, L., de Garidel-Thoron, T., Mix, A.C., Pisias, N.G., 2001. ENSO-like forcing on oceanic primary production during the Late Pleistocene. Science 293, 2440–2444.
Beaufort, L., de Garidel-Thoron, T., Linsley, B., Oppo, D., Buchet, N., 2003. Biomass burning and oceanic primary production estimates in the Sulu Sea area over the last 380 Ky and the East Asian monsoon dynamics. Marine Geology 201, 53–65.
Boeckel, B., Baumann, K.-H., 2004. Distribution of coccoliths in surface sediments of the south-eastern South Atlantic Ocean: ecology, preservation and carbonate contribution. Marine Micropaleontology 51, 301–320.
Bollmann, L., Baumann, K.-H., Thierstein, H.R., 1998. Global dominance of *Gephyrocapsa* coccoliths in the Late Pleistocene: selective dissolution, evolution or global environment change? Paleoceanography 13, 517–529.
Brand, L.E., 1994. Physiological ecology of marine coccolithophores. In: Winter, A., Siesser, A. (Eds.), Coccolithophores. Cambridge University Press, Cambridge, U.K., pp. 39–49.
Cachao, M., Moita, M.T., 2000. *Coccolithus pelagicus*, a productivity proxy related to moderate fronts off Western Iberia. Marine Micropaleontology 39, 131–155.
Chavez, F.P., Barber, R.T., 1987. An estimate of new production in the equatorial Pacific. Deep-Sea Research Part A, 34, 1229–1243.
Clement, A.C., Seager, R., Cane, M.A., 1999. Orbital controls on the El Niño/Southern Oscillation and the tropical climate. Paleoceanography 14, 441–456.
Droxler, A.W., Alley, R.B., Howard, W.R., Poore, R.Z., Burckle, L.H., 2003. Unique and exceptionally long interglacial marine isotope stage 11: window into Earth warm future climate. In: Droxler, A.W., Poore, R.Z., Burckle, L.H. (Eds.), Earth's Climate and Orbital Eccentricity. The Marine Isotope Stage 11 Question. . Monograph Series, vol. 137. AGU, Washington, DC, pp. 1–14.
Emeis, K.-C., Doose, H., Mix, A., Schulz-Bull, D., 1995. In: Pisias, N.G., Mayer, L.A., Janecek, T.R., Palmer-Julson, A., van Andel, T.H. (Eds.), Alkenone Sea Surface Temperatures and Carbon Burial at Site 846 (Eastern Equatorial Pacific Ocean): the Last 1.3 M.y. Proc. ODP, Sci. Results, vol. 138. Ocean Drilling Program, College Station, TX, pp. 605–613.
Farrell, J.W., Murray, D.W., McKenna, V.S., Ravelo, A.C., 1995. In: Pisias, N.G., Mayer, L.A., Janecek, T.R., Palmer-Julson, A., van Andel, T.H. (Eds.), Upper Ocean Temperature and Nutrient Contrast Inferred from Pleistocene Planktonic Foraminifer $\delta^{18}O$ and $\delta^{13}C$ in the Eastern Equatorial Pacific. Proc. ODP, Sci. Results, vol. 138. Ocean Drilling Program, College Station, TX, pp. 289–319.
Fedorov, A.V., Philander, G., 2000. Is El Niño changing? Science 288, 1197–2002.
Fiedler, P.C., Talley, L.D., 2006. Hydrography of the eastern tropical Pacific: a review. Progress in Oceanography 69, 143–180.
Flores, J.A., Sierro, F.J., 1997. Revised technique for calculation of calcareous nannofossil accumulation rates. Micropaleontology 43, 321–324.
Flores, J.A., Gersonde, R., Sierro, F.J., 1999. Pleistocene fluctuations in the Agulhas current retroflection based on the calcareous plankton record. Marine Micropaleontology 37, 1–22.
Flores, J.A., Bárcena, M.A., Sierro, F.J., 2000. Ocean-surface and wind dynamics in the Atlantic Ocean off Northwest Africa during the last 140 000 years. Palaeogeography, Palaeoclimatology, Palaeoecology 161, 459–478.
Flores, J.A., Marino, M., Sierro, F.J., Hodell, D.A., Charles, C.D., 2003. Calcareous plankton dissolution pattern and coccolithophore assemblages during the last 600 kyr at ODP Site 1089 (Cape Basin, South Atlantic): paleoceanographic implications. Palaeogeography, Palaeoclimatology, Palaeoecology 196, 409–426.
Flores, J.-A., Wei, W., López-Otálvaro, G.E., Alvarez, C., Sierro, F.J., 2006. In: Tiedemann, R., Mix, A.C., Richter, C., Ruddiman, W.F. (Eds.), Data Report: Tropical and Equatorial Calcareous Nannofossil Pleistocene Biostratigraphy, ODP Leg 202. Proc. ODP, Sci. Results, vol. 202. College Station, TX, Ocean Drilling Program, pp. 1–10. doi:10.2973/odp.proc.sr.202.214.2006.
Geitzenauer, K.R., Roche, M.B., McIntyre, A., 1977. In: Ramsay (Ed.), Coccolithophore Biogeography of the North Atlantic and Pacific Surface Sediments. Oceanic Micropaleontology. Academic Press, New York, pp. 973–1008.
Giraudeau, J., 1992. Distribution of Recent nannofossils beneath the Benguela system: Southwest African continental margin. Marine Geology 108, 219–237.
Giraudeau, J., Monteiro, P.M.S., Nikodemus, K., 1993. Distribution and malformation of living coccolithophores in the northern Benguela upwelling system of Namibia. Marine Micropaleontology 22, 93–110.
Hagelberg, T.K., Pisias, N.G., Mayer, L.A., Shckleton, N.J., Mix, A.C., 1995. In: Pisias, N.G., Mayer, L.A., Janecek, T.R., Palmer-Julson, A., van Andel, T.H. (Eds.), Spatial Variability of Late Neogene Equatorial Pacific Carbonate: Leg 138. Proc. ODP, Sci. Results, vol. 138. Ocean Drilling Program, College Station, TX, pp. 321–336.
Hagino, K., Okada, H., 2004. Floral response of coccolithophores to progressive oligotrophication in the South Equatorial Current, Pacific Ocean. In: Shiyomi, M., Kawahata, H., Koizumi, H., Tsuda, A., Awaya, Y. (Eds.), Global Environmental Change in the Ocean and on Land. TERRAPUB, pp. 121–132.
Helly, J., Levin, L., 2004. Global distribution of naturally occurring marine hypoxia on continental margins. Deep-Sea Research I 51, 1159–1168.
Hoffman, E.E., Busalacchi, A.J., O'Brien, J.J., 1981. Wind generation of the Costa Rica Dome. Science 214, 552–554.
Houghton, S.D., Guptha, M.V.S., 1991. Monsoonal and fertility controls on Recent marginal sea and continental shelf coccolith assemblages from the western Pacific and northern Indian oceans. Marine Geology 97, 251–259.
Hovan, S.A., 1995. In: Pisias, N.G., Mayer, L.A., Janecek, T.R., Palmer-Julson, A., van Andel, T.H. (Eds.), Late Cenozoic Atmospheric Circulation Intensity and Climatic History Recorded by Eolian Deposition in the Eastern Equatorial Pacific Ocean, Leg 138. Proc. ODP, Sci. Results, vol. 138. Ocean Drilling Program, College Station, TX, pp. 615–625.
Jansen, J.H.F., Kuijpers, A., Troelstra, S.R., 1986. A mid-Brunhes climatic event: long-term changes in global atmospheric and ocean circulation. Science 232, 619–622.
Kessler, W.S., 2006. The circulation of the eastern tropical Pacific: A review. Progress in Oceanography 69, 181–217.
Lea, D.W., Pak, D.K., Belanger, C.L., Spero, H.J., Hall, M.A., Shackleton, N.J., 2006. Paleoclimate history of Galápagos surface waters over the last 135,000 yr. Quaternary Science Reviews 25, 1152–1157.
Liu, Z., Herbert, T., 2004. High-latitude on the Eastern Equatorial Pacific climate in the early Pleistocene epoch. Nature 427, 720–723.
Lukas, R., 1986. The termination of the Equatorial Undercurrent in the Eastern Pacific. Progress in Oceanography 16, 63–90.
Lyle, M., Murray, D.W., Finney, B.P., Dymond, J., Robbins, J.M., Brooksforce, K., 1988. The record of Late Pleistocene biogenic sedimentation in the eastern tropical Pacific Ocean. Paleoceanography 3, 39–59.
Lyle, M., Mix, A., Pisias, N., 2002. Patterns of $CaCO_3$ deposition in the eastern tropical Pacific Ocean for the last 150 kyr: evidence for a southeast Pacific depositional spike during marine isotope stage (MIS) 2. Paleoceanography 17 (2), 1013. doi:10.1029/2000PA000538.
Martínez, I., Rincón, D., Yokoyama, Y., Barrows, T., 2005. Foraminifera and coccoloithophorid assemblage changes in the Panama Basin during the last deglaciation: response to sea-surface productivity induced by a transient climate change. Palaeogeography, Palaeoclimatology, Palaeoecology 234, 114–126.
Mitchell-Innes, B.A., Winter, A., 1987. Coccolithophores: a major phytoplankton component in mature upwelled waters off Cape Peninsula, South Africa in March, 1983. Marine Biology 95, 25–30.
Mix, A.C., Tiedemann, R., Blum, P., et al., 2003. Proc. ODP, Init. Repts., vol. 202. Ocean Drilling Program, College Station, TX. doi:10.2973/odp.proc.ir.202.2003.
Molfino, B., McIntyre, A., 1990a. Nutricline variation in the equatorial Atlantic coincident with the Younger Dryas. Paleoceanography 5, 997–1008.
Molfino, B., McIntyre, A., 1990b. Precessional forcing of nutricline dynamics in the equatorial Atlantic. Science 249, 766–769.
Murray, D.W., Farrel, J.W., McKenna, V., 1995. In: Pisias, N.G., Mayer, L.A., Janecek, T.R., Palmer-Julson, A., van Andel, T.H. (Eds.), Biogenic Sedimentation at Site 847, Eastern Equatorial Pacific Ocean, during the past 3 My. Proc. ODP, Sci. Results, vol. 138. Ocean Drilling Program, College Station, TX, pp. 429–459.
Okada, H., Honjo, S., 1973. The distribution of oceanic coccolithophorids in the Pacific. Deep-Sea Research 20, 355–374.

Okada, H., Honjo, S., 1975. Distribution of coccolithophores in marginal seas along the western Pacific ocean and in the Red Sea. Marine Biology 31 (3), 271–286.
Okada, H., McIntyre, A., 1979. Seasonal distributions of Modern coccolithophores in the western Atlantic ocean. Marine Biology 54, 319–328.
Okada, H., Wells, P., 1997. Late Quaternary nannofossil indicators of climate change in two deep-sea cores associated with the Leeuwin Current off Western Australia. Palaeogeography, Palaeoclimatology, Palaeoecology 131, 413–432.
Paillard, D.L., Labeyrie, L., Yiou, P., 1996. Macintosh program performs time-series analysis. EOS, Transactions, American Geophysical Union, 77 (39), 379.
Pak, H., Zaneveld, J.R., 1974. Equatorial Front in the eastern Pacific ocean. Journal of Physical Oceanography 4, 570–578.
Philander, G., 1995. El Niño and La Niña. In: Pirie, R.G. (Ed.), Oceanography: Contemporary Readings in Ocean Sciences, Oxford Univ. Press, Oxford, U.K., pp. 72–87.
Philander, S.G.H., Gu, D., Halpern, D., Lambert, G., Lau, N.-C., Li, T., Pacanowski, R.C., 1996. Why the ITCZ is mostly north of the Equator. Journal of Climate 9, 2958–2972.
Ravelo, A.C., Shackleton, N.J., 1995. In: Pisias, N.G., Mayer, L.A., Janecek, T.R., Palmer-Julson, A., van Andel, T.H. (Eds.), Evidence for Surface Water Circulation Changes at ODP Site 851 in the Eastern Tropical Pacific. Proc. ODP, Sci. Results, vol. 138. Ocean Drilling Program, College Station, TX, pp. 503–514.
Rickaby, R.E.M., Halloran, P., 2005. Cool La Niña during the warmth of the Pliocene? Science 307, 1948–1952.
Scharmm, C.T., 1985. Implications of radiolarian assemblages for the Late Quaternary Paleoceanography of the eastern equatorial Pacific. Quaternary Research 25, 204–218.
Shackleton, N.J., Berger, A., Peltier, W.R., 1990. An alternative astronomical calibration of the Pleistocene timescale based on ODP Site 677. Transactions of the Royal Society of Edinburgh: Earth Sciences 81, 251–261.
Smith, W.H.F., Sandwell, D.T., 1997. Global sea floor topography from satellite altimetry and ship depth soundings. Science 277, 1956–1962.
Snoeckx, H., Rea, D., 1994. Late Quaternary $CaCO_3$ stratigraphy of the eastern equatorial Pacific. Paleoceanography 9 (2), 341–352.
Thierstein, H.R., Geitzenauer, K.R., Molfino, B., Shackleton, N.J., 1977. Global synchroneity of late Quaternary coccolith datum levels: validation by oxygen isotopes. Geology 5, 400–404.
Thomas, E., Turekian, K.K., Wei, K.-Y., 2000. Productivity control of fine particle transport to equatorial Pacific. Global Biogeochemical Cycles 14, 945–955.
Weber, M.E., 1998. Estimation of biogenic carbonate and opal by continuous non-destructive measurements in deep-sea sediments: application to the Eastern Equatorial Pacific. Deep-Sea Research I 45, 1955–1975.
Wells, P., Okada, H., 1997. Response of nannoplankton to major changes in sea-surface temperature and movements of hydrological fronts over Site DSDP 594 (south Chatham Rise, southeastern New Zealand), during the last 130 kyr. Marine Micropaleontology 32, 341–363.
Winter, A., 1982. Paleoenvironmental interpretation of Quaternary coccolith assemblages from the Gulf of Aquaba (Elat), Red Sea. Revista Española de Micropaleontología 14, 291–314.
Wyrtki, K., 1981. An estimate of equatorial upwelling in the Pacific. Journal of Physical Oceanography 11, 1205–1214.
Young, J.R., 1994. Functions of coccoliths. In: Winter, A., Siesser, W.G. (Eds.), Coccolithophores. Cambridge Univ. Press, Cambridge, U.K., pp. 63–82.
Young, J.R., Ziveri, P., 2000. Calculation of coccolith volume and its use in calibration of carbonate flux estimates. Deep-Sea Research A 47, 1679–1700.